

# Quantum topological phase transitions in skyrmion crystals

Kristian Mæland and Asle Sudbø\*

Center for Quantum Spintronics, Department of Physics, Norwegian University of Science and Technology, NO-7491 Trondheim, Norway

Topological order is important in many aspects of condensed matter physics, and has been extended to bosonic systems. In this Letter we report the non-trivial topology of the magnon bands in two distinct quantum skyrmion crystals appearing in zero external magnetic field. This is revealed by nonzero Chern numbers for some of the bands. As a bosonic analog of the quantum anomalous Hall effect, we show that topological magnons can appear in skyrmion crystals without explicitly breaking time reversal symmetry with an external magnetic field. By tuning the value of the easy-axis anisotropy at zero temperature, we find eight quantum topological phase transitions signaled by discontinuous jumps in certain Chern numbers. We connect these quantum topological phase transitions to gaps closing and reopening between magnon bands.

*Introduction.* Topological order in fermionic condensed matter systems lies at the heart of the understanding of the quantum Hall effect (QHE) [1, 2], the quantum anomalous Hall effect (QAHE) [3, 4], the quantum spin Hall effect (QSHE) [5], and topological insulators (TIs) [6]. The QHE involves explicit time reversal symmetry breaking by an external magnetic field, while the QSHE and TIs are found in time-reversal-symmetric systems [5–8]. The QAHE is a special case, where the model is time reversal symmetric, but the system itself spontaneously breaks time reversal symmetry. It is a manifestation of the QHE without the need for an external magnetic field [4]. It was later shown that also bosonic excitations may feature topological properties [9–12]. The collective fluctuations of quantum spins, i.e., magnons, have been shown to be topologically non-trivial in magnonic crystals [9], dipolar magnetic thin films [10], and in ferromagnets on the honeycomb lattice [13–17]. In the model used in Refs. [13–15], next-nearest neighbor Dzyaloshinskii-Moriya interaction (DMI) realizes a bosonic analog of the Haldane model [3] in a system of insulating spins.

Even though analogies have been proposed [13, 17–20], topological magnon systems do not show direct equivalences of the QHE, QAHE, and QSHE [5, 6, 15]. Since bosons obey Bose-Einstein rather than Fermi-Dirac statistics, the Hall conductivity is not quantized [15]. Ref. [11] introduces the bosonic analog of a TI, a topological magnon insulator. The non-trivial topology of the magnon bands gives rise to chiral edge states within a bulk magnon gap. However, since bosonic systems lack the concept of a Fermi surface, the bulk is not guaranteed to be insulating with respect to spin currents [14]. Still, the chiral edge states resulting from topologically non-trivial magnons allow the creation of magnon currents that are insensitive to backscattering and disorder [9, 10]. These hold promising applications such as spin-current splitters, waveguides, and interferometers [9, 12]. In addition, magnetoelastic coupling leads to chiral phonon transport induced by the topological magnons [15].

The non-trivial real space magnetic texture of skyrmions means they are topologically protected [21, 22]. Therefore, skyrmions have received a great deal of interest, and are being explored for applications in magnetic memory technol-

ogy, unconventional computing, and numerous other applications [22–35]. The reciprocal space topology held by the magnon bands in skyrmion crystals (SkXs) has also been explored [36–40], and a topological phase transition driven by a magnetic field was found in Ref. [38]. Furthermore, evidence of the non-trivial topology of magnon bands in SkXs has been observed in an experiment [40].

In this Letter we reveal eight quantum topological phase transitions (QTPTs) [7, 41–43] driven by a tunable easy-axis anisotropy in the same SkXs that were explored in Ref. [44]. These QTPTs are signaled by discontinuous jumps in the Chern numbers [9] of the magnon bands. Here, we consider QTPTs to be topological phase transitions occurring at zero temperature by tuning a parameter in the Hamiltonian. The SkXs we consider are inspired by the observation of a SkX containing nanometer sized skyrmions in a magnetic monolayer [45]. Since the SkXs are stabilized in zero external magnetic field [44, 45], the QTPTs occur in a time-reversal-symmetric model. Instead, the magnetic order of the SkX ground state (GS) spontaneously breaks time reversal symmetry, allowing nonzero Chern numbers [12]. In that sense, our skyrmion system is more analogous to the QAHE in fermionic systems than previous studies of topological magnons in SkXs, where time reversal symmetry is explicitly broken by external magnetic fields [36–40].

As pointed out in Ref. [37], the bulk-edge correspondence is not guaranteed unless the finite geometry contains an integer number of unit cells. However, by letting the GS adapt to a strip geometry, Refs. [36–38] found the expected number and chirality [9] of edge states based on the bulk Chern numbers in SkXs. Therefore, we will not explicitly prove the existence of chiral edge states here. Assuming the validity of the bulk-edge correspondence in a finite geometry, the QTPTs could be used to switch chiral edge states on and off.

*Model.* As in Ref. [44], we use the time-reversal-symmetric Hamiltonian

$$H = H_{\text{ex}} + H_{\text{DM}} + H_{\text{A}} + H_4, \quad (1)$$

where

$$H_{\text{ex}} = -J \sum_{\langle ij \rangle} \mathbf{S}_i \cdot \mathbf{S}_j, \quad (2)$$

$$H_{\text{DM}} = \sum_{\langle ij \rangle} D_{ij} \cdot (\mathbf{S}_i \times \mathbf{S}_j), \quad (3)$$

\* Corresponding author: asle.sudbo@ntnu.no

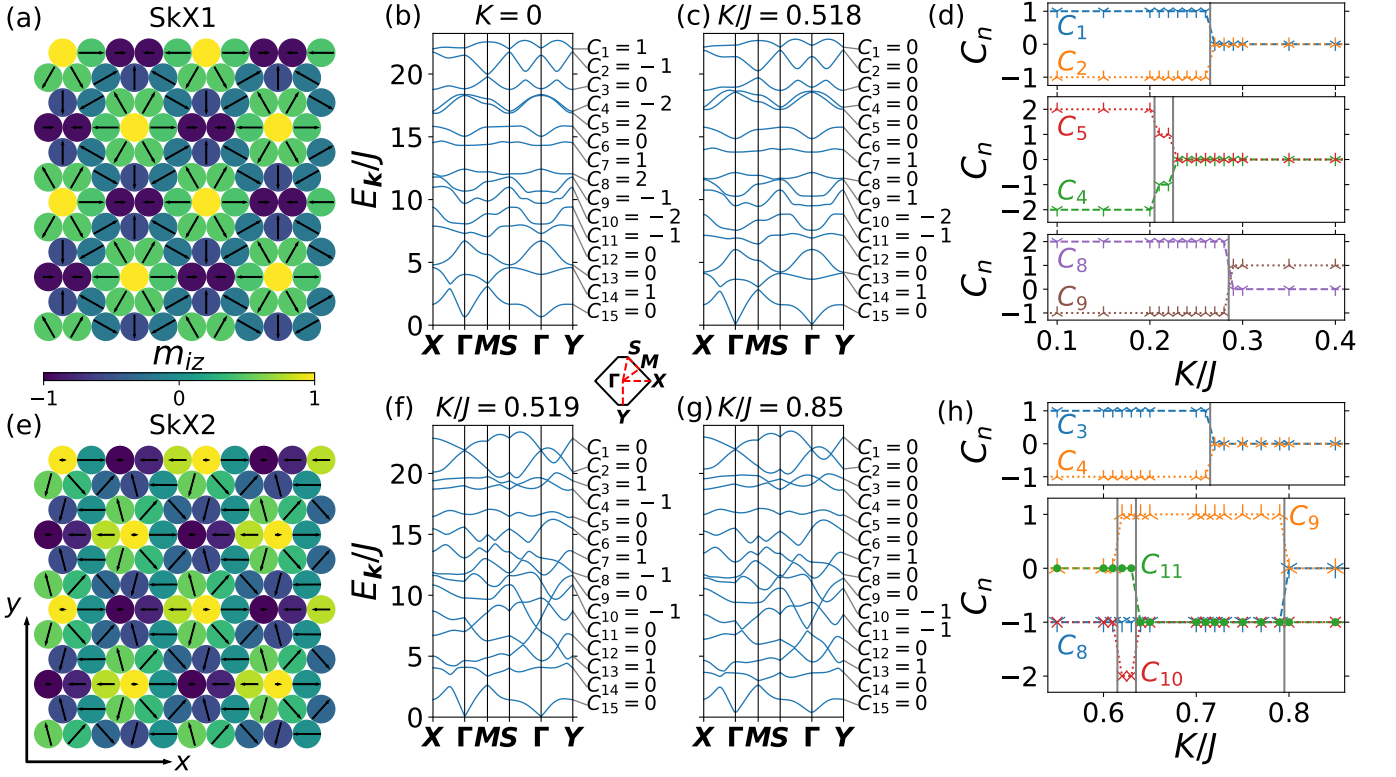


FIG. 1. (a) The classical ground state of the skyrmion crystal SkX1, (b) its magnon spectrum at low  $K$  along with the Chern numbers of each band, and (c) its magnon spectrum at high  $K$  along with the Chern numbers of each band. The spectra are plotted along the path in the first Brillouin zone (1BZ) that is sketched in the middle. (d) Shows the four quantum topological phase transitions (QTPTs) found in SkX1, where some Chern numbers show discontinuous jumps at the approximate values of  $K/J$  shown in gray. The calculated Chern numbers are shown with markers, while dotted or dashed lines are included for illustration. (e-h) The same as (a-d) but for the distinct skyrmion crystal SkX2. The parameters are  $D/J = 2.16$ ,  $U/J = 0.35$ ,  $S = 1$ , (a)  $K/J = 0.518$ , and (e)  $K/J = 0.519$ .

$$H_A = -K \sum_i S_{iz}^2, \quad (4)$$

$$H_4 = U \sum_{ijkl} [(S_i \cdot S_j)(S_k \cdot S_l) + (S_i \cdot S_l)(S_j \cdot S_k) - (S_i \cdot S_k)(S_j \cdot S_l)]. \quad (5)$$

The spin operator  $S_i$  with magnitude  $S$  pertains to lattice site  $i$  on the triangular lattice. We consider nearest neighbor ferromagnetic exchange interaction,  $J > 0$ . In Ref. [45], DMI between Fe atoms on the surface originates with the strong spin-orbit coupling from the Ir atoms [23]. We assume a similar effect in our model and set the DMI vector to  $D_{ij} = D\hat{r}_{ij} \times \hat{z}$ , where  $\hat{r}_{ij}$  is a unit vector from site  $i$  to site  $j$ . Like in Ref. [44], we will discuss a tunable easy-axis anisotropy,  $K$ , motivated by Refs. [46, 47] where it was shown that applying mechanical strain can tune the magnetic anisotropy. The Hamiltonian also contains the four-spin interaction  $H_4$ , acting between four sites that are oriented counterclockwise and make diamonds of minimal area [45, 48]. The reduced Planck's constant  $\hbar$  and the lattice constant  $a$  are set to one.

We refer to Ref. [44] for details of the two distinct SkX GSs, which are separated by a quantum phase transition

(QPT) at  $K = K_t$  with  $K_t/J \in (0.518, 0.519)$ . The classical GSs of SkX1 and SkX2 are shown in Fig. 1(a,e) for  $K/J = 0.518$  and  $K/J = 0.519$ , respectively. There,  $m_{iz}$  is the  $z$  component of the unit vector determining the direction of the spin at site  $i$ . We reiterate that it is the quantum skyrmions which are the preferred states of the system, not their corresponding classical GSs [44]. The introduction of the Holstein-Primakoff transformation via rotated coordinates [49] involves approximations whose validity were discussed in Ref. [44]. Possible corrections to our predictions due to the ignored magnon-magnon interactions are discussed in Refs. [12, 37]. The diagonalization of the system to obtain the magnon bands [50] was shown in detail in Ref. [44]. We take the transformation matrices  $T_k$ , and the magnon bands  $E_{k,n}$  as inputs in this Letter. The 15 magnon bands are numbered from top to bottom in terms of energy. The first Brillouin zone (1BZ) is the same for all 15 sublattices in both SkX1 and SkX2 and we define the points  $\Gamma = (0, 0)$ ,  $X = (52\pi/135, 0)$ ,  $M = (\pi/5, \pi/3\sqrt{3})$ ,  $S = (2\pi/135, 2\pi/3\sqrt{3})$ , and  $Y = (0, -2\pi/3\sqrt{3})$  in the 1BZ [44]. These points and the 1BZ are sketched in Fig. 1.

*Chern numbers.* Let  $\Gamma_n$  be a matrix whose  $n$ th diagonal element is 1 and all other matrix elements are zero,  $\Gamma_{n,i,j} = \delta_{in}\delta_{jn}$ . From this, we define a projection matrix

$P_{\mathbf{k},n} = T_{\mathbf{k}}^{-1} \Gamma_n T_{\mathbf{k}}$ . The bosonic nature of the magnons is encoded in the paraunitary transformation matrix [44, 50]. Then, the Berry curvature of the  $n$ th band is given by [2, 9]

$$B_n(\mathbf{k}) = i\epsilon_{\mu\nu} \text{Tr}[(\delta_{k_\mu} P_{\mathbf{k},n}) P_{\mathbf{k},n} (\delta_{k_\nu} P_{\mathbf{k},n})], \quad (6)$$

where  $\epsilon_{\mu\nu}$  is the Levi-Civita tensor and  $\mu, \nu \in \{x, y\}$ . The Chern number of the  $n$ th band is its Berry curvature integrated over the 1BZ

$$C_n = \frac{1}{2\pi} \int_{\text{1BZ}} d\mathbf{k} B_n(\mathbf{k}). \quad (7)$$

It can be shown that the Chern numbers are integers, given that the bands are isolated [9]. Here, we calculate the Chern numbers using numerical approximations to the integral. We consider equally spaced discretizations and adaptive quadratures [51]. When the numerical results are found to approach integers upon increasing the density of  $\mathbf{k}$  points, we present the Chern numbers as integers.

*Quantum topological phase transitions.* In Fig. 1(b,c) we show the magnon spectrum in SkX1 for  $K = 0$  and for  $K/J = 0.518$ , i.e., close to the QPT to SkX2. The Chern numbers of the 15 bands are given at both values of  $K$  and it is clear some of them have changed due to the change in easy-axis anisotropy. In Fig. 1(d) we plot these as a function of  $K$ , revealing four QTPTs.  $E_{\mathbf{k},4}$  and  $E_{\mathbf{k},5}$  first cross at the  $\mathbf{Y}$  point for the specific value  $K = K_1$ , where  $K_1/J$  is in the interval  $(0.20, 0.21)$ . They also cross at the  $\Gamma$  point for  $K/J = K_2/J \in (0.22, 0.23)$ . The gap between the bands closes and reopens, and their Chern numbers change, signaling QTPTs.  $E_{\mathbf{k},1}$  and  $E_{\mathbf{k},2}$  cross at the  $\mathbf{Y}$  point for  $K/J = K_3/J \in (0.26, 0.27)$ . The two Chern numbers annihilate, and both bands are topologically trivial for  $K > K_3$ . Finally, the gap between  $E_{\mathbf{k},8}$  and  $E_{\mathbf{k},9}$  closes between the  $\Gamma$  point and the  $\mathbf{X}$  point for  $K/J = K_4/J \in (0.28, 0.29)$ . Only  $E_{\mathbf{k},9}$  remains topologically non-trivial when the gap reopens for  $K > K_4$ . In SkX1, the magnon band with lowest energy is topologically trivial, while the band with second lowest energy is topologically non-trivial. For ferromagnetic SkXs in an external magnetic field, the band with third lowest energy is topologically non-trivial while the two bands with lower energy are topologically trivial [36, 38–40].

Fig. 1(e,f) shows the magnon spectrum in SkX2 for  $K/J = 0.519$  and  $K/J = 0.85$ . Despite the plethora of closely avoided crossings, all the bands are isolated at these values of  $K$ , and all 15 Chern numbers are well defined. Notice that in all cases the sum of the Chern numbers of all bands is zero, as expected [9]. It is clear that the Chern numbers have changed from the spectrum of SkX1 at  $K/J = 0.518$  to the spectrum of SkX2 at  $K/J = 0.519$ . We do not view this as a QTPT, since it is not due to gaps closing and reopening in the magnon spectrum. Rather, the magnon spectra are different from the outset, since they arise from two distinct SkXs [44].

In Fig. 1(g) we plot the Chern numbers that change when tuning  $K$  in SkX2. We find four QTPTs. The gap between  $E_{\mathbf{k},9}$  and  $E_{\mathbf{k},10}$  closes between  $\Gamma$  and  $\mathbf{Y}$  for  $K/J = K_5/J \in (0.61, 0.62)$ . Once the gap reopens,  $E_{\mathbf{k},9}$  has become topologically non-trivial, while  $C_{10} = -1$  has jumped

to  $C_{10} = -2$ .  $E_{\mathbf{k},10}$  and  $E_{\mathbf{k},11}$  cross between  $\Gamma$  and  $\mathbf{Y}$  for  $K/J = K_6/J \in (0.63, 0.64)$ .  $C_{10}$  jumps back to  $-1$ , allowing  $E_{\mathbf{k},11}$  to become topologically non-trivial for  $K > K_6$ . The gap between  $E_{\mathbf{k},3}$  and  $E_{\mathbf{k},4}$  closes between  $\Gamma$  and  $\mathbf{Y}$  for  $K/J = K_7/J \in (0.71, 0.72)$ . Once the gap reopens at  $K > K_7$  they are both topologically trivial. Finally,  $E_{\mathbf{k},8}$  and  $E_{\mathbf{k},9}$  cross at  $\mathbf{k} \approx (\pm 0.32, 0.10)$  for  $K/J = K_8/J \in (0.79, 0.80)$  and are left topologically trivial for  $K > K_8$ .

*Gap closing and Berry curvature.* In Fig. 2(a) we go into detail of the two band crossings of  $E_{\mathbf{k},4}$  and  $E_{\mathbf{k},5}$  in SkX1. For  $K < K_1$  we have  $C_4 = -2, C_5 = 2$ . Then, at  $K = K_1$  the gap between  $E_{\mathbf{k},4}$  and  $E_{\mathbf{k},5}$  at the  $\mathbf{Y}$  point closes,  $\Delta_{4,5}^{\mathbf{Y}} = 0$ , and the two Chern numbers are undefined [9]. For  $K > K_1$  the gap reopens and  $C_4 = -1, C_5 = 1$ , i.e., the bands remain topologically non-trivial. For  $K = K_2$  the gap closes at the  $\Gamma$  point,  $\Delta_{4,5}^{\Gamma} = 0$ . When the gap reopens for  $K > K_2$  both bands have become topologically trivial. The dependence of these two gaps on the easy-axis anisotropy is shown in Fig. 2(b). It appears the two gaps close with an approximately linear dependence on  $K$ .

The Berry curvatures of  $E_{\mathbf{k},4}$  and  $E_{\mathbf{k},5}$  are shown in Fig. 2(c). At  $K = 0$ ,  $B_4(\mathbf{k})$  has extended negative valleys, giving rise to a negative Chern number. For  $K/J = 0.22$ ,  $\Delta_{4,5}^{\Gamma}$  is small and so there is a sharp negative valley in  $B_4(\mathbf{k})$  around  $\mathbf{k} = \Gamma$ . Again, this gives rise to a negative Chern number. At  $K/J = 0.3$ , the Berry curvature contains both positive peaks and negative valleys, which cancel each other out in the integral and lead to zero Chern number. The arguments are similar for  $B_5(\mathbf{k})$  and  $C_5$ . From these figures, it is clear that the gap closings involve an exchange of Berry curvature between the bands. Also, the Berry curvature of a given band has its largest absolute values where the band has the smallest gap to neighboring bands. Similar figures and arguments can be extended to the remaining six QTPTs discussed in this Letter. Notice that each time two bands cross and undergo a QTPT, the sum of their Chern numbers is preserved, as expected [2].

*Predicted edge states.* The predicted number of edge states within the gap between the bands  $E_{\mathbf{k},n}$  and  $E_{\mathbf{k},n+1}$  is

$$\nu_n = \sum_{n'=n+1}^{15} C_{n'}. \quad (8)$$

The chiral edge states propagate clockwise (counterclockwise) for positive (negative)  $\nu_n$  [9]. For instance, we predict a clockwise edge state within the bulk band gap between  $E_{\mathbf{k},13}$  and  $E_{\mathbf{k},14}$  in SkX1. Let SkX3 be the result of applying the time-reversal operator, i.e., flipping all spins, to SkX1. In Ref. [44], we mentioned that since the Hamiltonian in Eq. (1) is time-reversal symmetric, SkX1 and SkX3 are degenerate in energy. It was also mentioned that the two states can appear concurrently, separated by domain walls. SkX3 has the same magnon spectrum as SkX1, while the Chern numbers change sign. At the interface between two topologically non-trivial systems  $A$  and  $B$ , with  $\nu_n = \nu_A$  and  $\nu_n = \nu_B$  in the same energy interval, one expects  $|\nu_A - \nu_B|$  edge states [36]. Therefore, along a domain wall between SkX1 and SkX3, we predict two chiral edge states within the gap between  $E_{\mathbf{k},13}$  and  $E_{\mathbf{k},14}$ .

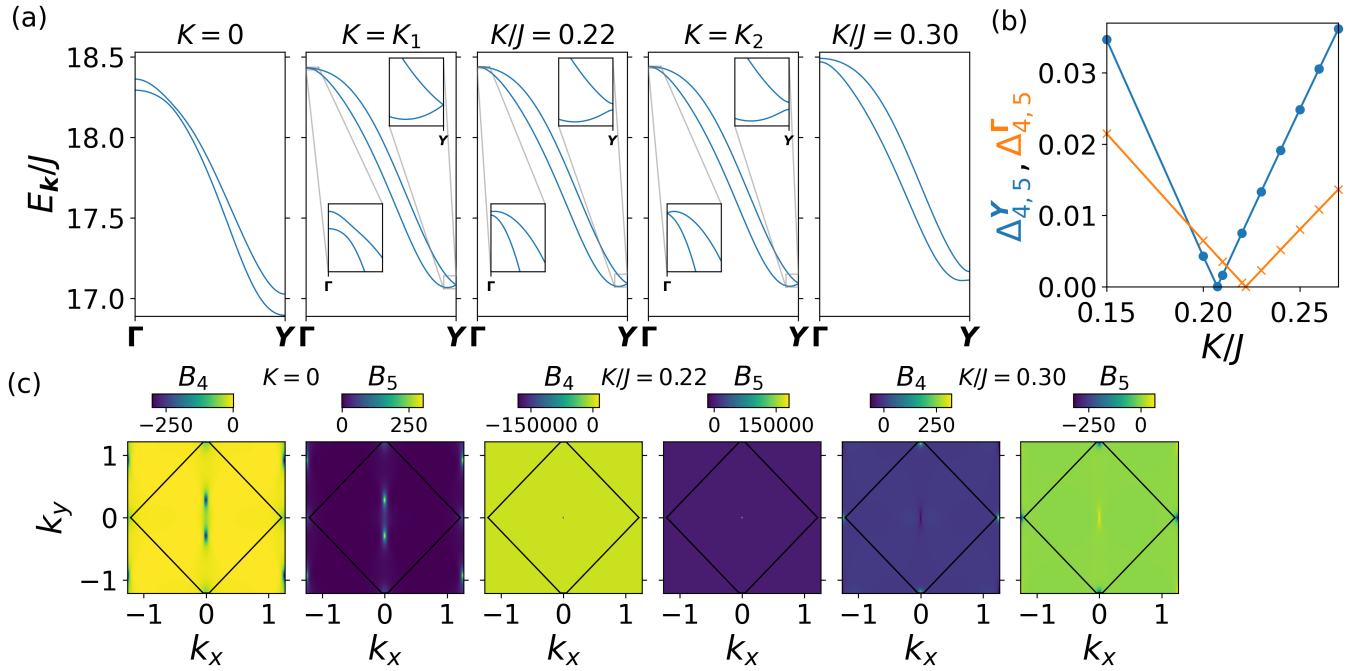


FIG. 2. (a) Plots of  $E_{k,4}$  and  $E_{k,5}$  in SkX1 at varying  $K$  showing how the gap at  $Y$  closes at  $K = K_1$  where there is a QTPT and  $C_4 = -2, C_5 = 2$  at  $K < K_1$  goes to  $C_4 = -1, C_5 = 1$  at  $K_1 < K < K_2$  once the gap reopens. Also, the gap closes at the  $\Gamma$  point for  $K = K_2$ , and once it reopens, the two bands are topologically trivial. (b) The gap between  $E_{k,4}$  and  $E_{k,5}$  at the  $Y$  ( $\Gamma$ ) point is shown in blue (orange), with circles (crosses) at the calculated values. (c) The Berry curvatures of bands  $E_{k,4}$  and  $E_{k,5}$  shown for the three values of  $K$  in (a) where the bands are isolated. The 1BZ is indicated in black and the Berry curvatures are plotted with 201 points in each direction. The parameters are  $D/J = 2.16, U/J = 0.35$ , and  $S = 1$ .

*Details of Chern number calculation.* As shown in Fig. 2(c), the Berry curvature develops strong peaks or valleys at values of  $\mathbf{k}$  where the band has closely avoided crossings with other bands. This presents a numerical challenge in calculating the integral of the Berry curvature over the 1BZ. This is especially a challenge in SkX2, where many bands have closely avoided crossings at all values of  $K/J$ . We used the recursive algorithm in Ref. [51] to obtain adaptive quadratures, where the density of  $\mathbf{k}$  values is largest around the sharp peaks and valleys. In general, this gave accurate numerical results, with deviations from integer Chern numbers decreasing to  $\mathcal{O}(10^{-5})$  or better with increasing number of  $\mathbf{k}$  points in the quadrature.

For  $K/J = 0.71$  in SkX2,  $E_{k,3}$  and  $E_{k,4}$  are very close to crossing, with a gap of  $\mathcal{O}(10^{-7}J)$ . This yields extremely sharp peaks in the Berry curvatures and numerical difficulties led to  $C_3 \approx 0.995$  and  $C_4 \approx -0.995$  for both  $10^6$  and  $10^7$   $\mathbf{k}$  points in the adaptive quadrature. These are the greatest deviations from integers in our results. We view this as a numerical artifact since  $K/J = 0.71$  is very close to the value  $K = K_7$  where  $E_{k,3}$  and  $E_{k,4}$  cross. The numerical Chern numbers are better approximations of integers at values of  $K$  further away from  $K = K_7$  than  $K/J = 0.71$ .

The derivatives in the Berry curvature in Eq. (6) were calcu-

lated using forward difference with  $\Delta k_\mu = 10^{-8}$ . In the case of an evenly spaced discretization, the integral is converted to a sum via  $\int d\mathbf{k} = (A_{1BZ}/N') \sum_{\mathbf{k}}$ , where  $A_{1BZ}$  is the area of the 1BZ, and  $N'$  is the number of magnetic unit cells, i.e., the number of  $\mathbf{k}$  points in the sum.

*Conclusion.* We found eight quantum topological phase transitions in two distinct skyrmion crystals that are stabilized in a time-reversal-symmetric model. Time reversal symmetry is spontaneously broken by the magnetic ordering of the skyrmions, and therefore nonzero Chern numbers of the magnon bands are possible. This is a bosonic analog of the quantum anomalous Hall effect. The quantum topological phase transitions, driven by a tunable easy-axis anisotropy at zero temperature, are signaled by jumps in the Chern numbers. We illustrated how the closing and subsequent reopening of the gaps between magnon bands leads to these jumps in the Chern numbers, and how the Berry curvature depends on these gaps.

*Acknowledgments.* We acknowledge funding from the Research Council of Norway through its Centres of Excellence funding scheme, Project No. 262633, ‘‘QuSpin’’, and through Project No. 323766, ‘‘Equilibrium and out-of-equilibrium quantum phenomena in superconducting hybrids with antiferromagnets and topological insulators’’.

[1] D. J. Thouless, M. Kohmoto, M. P. Nightingale, and M. den Nijs, Quantized Hall Conductance in a Two-Dimensional Peri-

odic Potential, *Phys. Rev. Lett.* **49**, 405 (1982).

- [2] J. E. Avron, R. Seiler, and B. Simon, Homotopy and Quantization in Condensed Matter Physics, *Phys. Rev. Lett.* **51**, 51 (1983).
- [3] F. D. M. Haldane, Model for a Quantum Hall Effect without Landau Levels: Condensed-Matter Realization of the “Parity Anomaly”, *Phys. Rev. Lett.* **61**, 2015 (1988).
- [4] C.-X. Liu, S.-C. Zhang, and X.-L. Qi, The Quantum Anomalous Hall Effect: Theory and Experiment, *Annu. Rev. Condens. Matter Phys.* **7**, 301 (2016).
- [5] C. L. Kane and E. J. Mele,  $Z_2$  Topological Order and the Quantum Spin Hall Effect, *Phys. Rev. Lett.* **95**, 146802 (2005).
- [6] M. Z. Hasan and C. L. Kane, Colloquium: Topological insulators, *Rev. Mod. Phys.* **82**, 3045 (2010).
- [7] B. A. Bernevig, T. L. Hughes, and S.-C. Zhang, Quantum Spin Hall Effect and Topological Phase Transition in HgTe Quantum Wells, *Science* **314**, 1757 (2006).
- [8] J. E. Moore and L. Balents, Topological invariants of time-reversal-invariant band structures, *Phys. Rev. B* **75**, 121306 (2007).
- [9] R. Shindou, R. Matsumoto, S. Murakami, and J.-i. Ohe, Topological chiral magnonic edge mode in a magnonic crystal, *Phys. Rev. B* **87**, 174427 (2013).
- [10] R. Shindou, J.-i. Ohe, R. Matsumoto, S. Murakami, and E. Saitoh, Chiral spin-wave edge modes in dipolar magnetic thin films, *Phys. Rev. B* **87**, 174402 (2013).
- [11] L. Zhang, J. Ren, J.-S. Wang, and B. Li, Topological magnon insulator in insulating ferromagnet, *Phys. Rev. B* **87**, 144101 (2013).
- [12] P. A. McClarty, Topological Magnons: A Review, *Annu. Rev. Condens. Matter Phys.* **13**, 171 (2022).
- [13] S. K. Kim, H. Ochoa, R. Zarzuela, and Y. Tserkovnyak, Realization of the Haldane-Kane-Mele Model in a System of Localized Spins, *Phys. Rev. Lett.* **117**, 227201 (2016).
- [14] A. Rückriegel, A. Brataas, and R. A. Duine, Bulk and edge spin transport in topological magnon insulators, *Phys. Rev. B* **97**, 081106 (2018).
- [15] E. Thingstad, A. Kamra, A. Brataas, and A. Sudbø, Chiral Phonon Transport Induced by Topological Magnons, *Phys. Rev. Lett.* **122**, 107201 (2019).
- [16] S. A. Owerre, A first theoretical realization of honeycomb topological magnon insulator, *J. Phys. Condens. Matter* **28**, 386001 (2016).
- [17] H. Huang, T. Kariyado, and X. Hu, Topological magnon modes on honeycomb lattice with coupling textures, *Sci. Rep.* **12**, 1 (2022).
- [18] K. Nakata, J. Klinovaja, and D. Loss, Magnonic quantum Hall effect and Wiedemann-Franz law, *Phys. Rev. B* **95**, 125429 (2017).
- [19] K. H. Lee, S. B. Chung, K. Park, and J.-G. Park, Magnonic quantum spin Hall state in the zigzag and stripe phases of the antiferromagnetic honeycomb lattice, *Phys. Rev. B* **97**, 180401 (2018).
- [20] S. A. Owerre, Floquet topological magnons, *J. Phys. Commun.* **1**, 021002 (2017).
- [21] S.-G. Je, H.-S. Han, S. K. Kim, S. A. Montoya, W. Chao, I.-S. Hong, E. E. Fullerton, K.-S. Lee, K.-J. Lee, M.-Y. Im, and J.-I. Hong, Direct Demonstration of Topological Stability of Magnetic Skyrmions *via* Topology Manipulation, *ACS Nano* **14**, 3251 (2020).
- [22] N. Nagaosa and Y. Tokura, Topological properties and dynamics of magnetic skyrmions, *Nat. Nanotechnol.* **8**, 899 (2013).
- [23] G. Finocchio, F. Büttner, R. Tomasello, M. Carpentieri, and M. Kläui, Magnetic skyrmions: from fundamental to applications, *J. Phys. D: Appl. Phys.* **49**, 423001 (2016).
- [24] F. Jonietz, S. Mühlbauer, C. Pfleiderer, A. Neubauer, W. Münzer, A. Bauer, T. Adams, R. Georgii, P. Böni, R. A. Duine, K. Everschor, M. Garst, and A. Rosch, Spin Transfer Torques in MnSi at Ultralow Current Densities, *Science* **330**, 1648 (2010).
- [25] C. Back *et al.*, The 2020 skyrmionics roadmap, *J. Phys. D: Appl. Phys.* **53**, 363001 (2020).
- [26] R. Tomasello, E. Martinez, R. Zivieri, L. Torres, M. Carpentieri, and G. Finocchio, A strategy for the design of skyrmion racetrack memories, *Sci. Rep.* **4**, 1 (2014).
- [27] A. Fert, V. Cros, and J. Sampaio, Skyrmions on the track, *Nat. Nanotechnol.* **8**, 152 (2013).
- [28] V. V. Mazurenko, Y. O. Kvashnin, A. I. Lichtenstein, and M. I. Katsnelson, A DMI guide to magnets micro-world, *J. Exp. Theor. Phys.* **132**, 506 (2021).
- [29] E. A. Stepanov, C. Dutreix, and M. I. Katsnelson, Dynamical and Reversible Control of Topological Spin Textures, *Phys. Rev. Lett.* **118**, 157201 (2017).
- [30] E. A. Stepanov, S. A. Nikolaev, C. Dutreix, M. I. Katsnelson, and V. V. Mazurenko, Heisenberg-exchange-free nanoskyrmion mosaic, *J. Phys.: Condens. Matter* **31**, 17LT01 (2019).
- [31] N. Romming, C. Hanneken, M. Menzel, J. E. Bickel, B. Wolter, K. von Bergmann, A. Kubetzka, and R. Wiesendanger, Writing and Deleting Single Magnetic Skyrmions, *Science* **341**, 636 (2013).
- [32] P.-J. Hsu, A. Kubetzka, A. Finco, N. Romming, K. von Bergmann, and R. Wiesendanger, Electric-field-driven switching of individual magnetic skyrmions, *Nat. Nanotechnol.* **12**, 123 (2017).
- [33] G. Yu, P. Upadhyaya, Q. Shao, H. Wu, G. Yin, X. Li, C. He, W. Jiang, X. Han, P. K. Amiri, and K. L. Wang, Room-temperature skyrmion shift device for memory application, *Nano Lett.* **17**, 261 (2017).
- [34] X. Zhang, M. Ezawa, and Y. Zhou, Magnetic skyrmion logic gates: conversion, duplication and merging of skyrmions, *Sci. Rep.* **5**, 1 (2015).
- [35] C. Psaroudaki and C. Panagopoulos, Skyrmion Qubits: A New Class of Quantum Logic Elements Based on Nanoscale Magnetization, *Phys. Rev. Lett.* **127**, 067201 (2021).
- [36] A. Roldán-Molina, A. S. Nunez, and J. Fernández-Rossier, Topological spin waves in the atomic-scale magnetic skyrmion crystal, *New J. Phys.* **18**, 045015 (2016).
- [37] S. A. Díaz, J. Klinovaja, and D. Loss, Topological Magnons and Edge States in Antiferromagnetic Skyrmion Crystals, *Phys. Rev. Lett.* **122**, 187203 (2019).
- [38] S. A. Díaz, T. Hirokawa, J. Klinovaja, and D. Loss, Chiral magnonic edge states in ferromagnetic skyrmion crystals controlled by magnetic fields, *Phys. Rev. Res.* **2**, 013231 (2020).
- [39] J. Waizner, *Spin wave excitations in magnetic helices and skyrmion lattices*, *Ph.D. thesis*, Universität zu Köln (2016).
- [40] T. Weber, D. M. Fobes, J. Waizner, P. Steffens, G. S. Tucker, M. Böhm, L. Beddrich, C. Franz, H. Gabold, R. Bewley, D. Voneshen, M. Skoulatos, R. Georgii, G. Ehlers, A. Bauer, C. Pfleiderer, P. Böni, M. Janoschek, and M. Garst, Topological magnon band structure of emergent Landau levels in a skyrmion lattice, *Science* **375**, 1025 (2022).
- [41] C. Castelnovo and C. Chamon, Quantum topological phase transition at the microscopic level, *Phys. Rev. B* **77**, 054433 (2008).
- [42] A. Hamma, W. Zhang, S. Haas, and D. A. Lidar, Entanglement, fidelity, and topological entropy in a quantum phase transition to topological order, *Phys. Rev. B* **77**, 155111 (2008).
- [43] E. Samimi, M. H. Zarei, and A. Montakhab, Global entanglement in a topological quantum phase transition, *Phys. Rev. A*

- [105, 032438 \(2022\)](#).
- [44] K. Mæland and A. Sudbø, Quantum fluctuations in the chiral order parameter of quantum skyrmion crystals, [arXiv:2204.02999 \(2022\)](#).
- [45] S. Heinze, K. von Bergmann, M. Menzel, J. Brede, A. Kubetzka, R. Wiesendanger, G. Bihlmayer, and S. Blügel, Spontaneous atomic-scale magnetic skyrmion lattice in two dimensions, [Nat. Phys. 7, 713 \(2011\)](#).
- [46] L. Webster and J.-A. Yan, Strain-tunable magnetic anisotropy in monolayer CrCl<sub>3</sub>, CrBr<sub>3</sub>, and CrI<sub>3</sub>, [Phys. Rev. B 98, 144411 \(2018\)](#).
- [47] R. Albaridy, A. Manchon, and U. Schwingenschlögl, Tunable magnetic anisotropy in Cr-trihalide Janus monolayers, [J. Condens. Matter Phys. 32, 355702 \(2020\)](#).
- [48] A. H. MacDonald, S. M. Girvin, and D. Yoshioka,  $\frac{t}{U}$  expansion for the Hubbard model, [Phys. Rev. B 37, 9753 \(1988\)](#).
- [49] J. T. Haraldsen and R. S. Fishman, Spin rotation technique for non-collinear magnetic systems: application to the generalized Villain model, [J. Condens. Matter Phys. 21, 216001 \(2009\)](#).
- [50] J. H. P. Colpa, Diagonalization of the quadratic boson Hamiltonian, [Phys. A: Stat. Mech. Appl. 93, 327 \(1978\)](#).
- [51] S. E. Mousavi, J. E. Pask, and N. Sukumar, Efficient adaptive integration of functions with sharp gradients and cusps in  $n$ -dimensional parallelepipeds, [Int. J. Numer. Methods Eng. 91, 343 \(2012\)](#).